Chinese Chemical Letters 35 (2024) 109735

Contents lists available at ScienceDirect

Chinese Chemical Letters

journal homepage: www.elsevier.com/locate/cclet

Engineering aggregates of julolidine-substituted aza-BODIPY nanoparticles for NIR-II photothermal therapy

Lulu Cao[a,1], Yikun Li[b,1], Dongxiang Zhang[a], Shuai Yue[a], Rong Shang[c], Xin-Dong Jiang[a,*], Jianjun Du[b,*]

[a] Liaoning & Shenyang Key Laboratory of Functional Dye and Pigment, Shenyang University of Chemical Technology, Shenyang 110142, China
[b] State Key Laboratory of Fine Chemicals, Dalian University of Technology, Dalian 116024, China
[c] Department of Chemistry, Graduate School of Advanced Science and Engineering, Hiroshima University, Higashi-Hiroshima 7398526, Japan

ARTICLE INFO

Article history:
Received 24 December 2023
Revised 20 February 2024
Accepted 21 February 2024
Available online 8 March 2024

Keywords:
Aggregate
NIR-II
Julolidine
Aza-BODIPY
PTT

ABSTRACT

Near infrared-II (NIR-II) dyes have unique advantages in biomedical applications owing to the powerful ability in penetrating biological tissues. Herein, NIR-II aza-BODIPY dye, **QLD-BDP**, was developed with julolidine at 1,7-sites and *p*-dimethylaminophenyl group at 3,5-sites. According to X-ray analysis, **QLD-BDP** exhibits significant distortion, and this molecule appears a bowl shaped structure. The photothermal conversion efficiency of the self-assembled **QLD-BDP** nanoparticles (**QLD-BDP**-NPs) can reach 50.5%, with maximum emission at 998 nm by the aggregate. **QLD-BDP-**NPs can cause the complete destruction of 4T1 multicellular spheroids (MCSs), indicating a photothermal therapy (PTT) effect.

Near infrared (NIR) functional dyes, especially NIR-II (1000–1700 nm) dyes, have shown unique advantages in biomedical applications, due to their powerful ability in penetrating biological tissues [1–5]. Light in the NIR-II region can be strongly captured to transfer high photothermal conversion efficiencies (PCEs) for treating deep-seated tumors at deeper tissue penetration (~5–20 mm), because of the decreased tissue absorption, scattering and autofluorescence, compared to light in visible (400–700 nm) and NIR-I (700–900 nm) regions [6–16]. Therefore, the design and synthesis of NIR-II dyes have been attracting increasing interest.

In recent years, the classic molecule aza-borondipyrromethene (aza-BODIPY) has attracted the widespread attention, due to its excellent spectral properties such as high molar extinction coefficient [17–21]. However, owing to the limitation of the parent nucleus of aza-BODIPYs, their optical spectra rarely touch the NIR-II region [22–25]. The extension of the π-conjugated system and the wise selection of the donor groups are the effective ways to develop the NIR-II dye aza-BODIPY. Julolidine, with planarity and steric hindrance, is often used as a donor fragment for the star molecules in special fields such as functional dyes, chemical sensors, optoelectronic materials and so forth [26–29]. Recently, Li *et al.* introduced julolidine into the aza-BODIPY nucleus and prepared NIR-II dye **OMe-BDP** as template molecule for photothermal therapy (PTT) (Fig. 1a) [30]. Changing the donor groups at 3,5-sites to produce the remarkable red-shift of absorption maximum, NIR-II aza-BODIPY (**OMePh-BDP**) nanoparticles for efficient osteosarcoma PPT *via* concurrent apoptosis and pyroptosis were successfully constructed (Fig. 1a) [31]. Moreover, the metallacycle was obtained *via* the coordination driven self-assembly of the NIR-II fluorescent aza-BODIPY (**OMePY-BDP**) with di-pyridine at 2,6-sites as the ligand, which provided a paradigm for the development of long-wavelength emissive supramolecular theranostic agents based on ruthenium (Fig. 1a) [32]. However, there is no record for the structural chemistry and molecular aggregating state in the julolidine system. Therefore, we revealed its single crystal structure for the first time and further elucidated the aggregating state of julolidine-based aza-BODIPY. Powerful donor-acceptor (D-A) type molecule was smartly designed through the construction of 1,7-jiuluolidine-3,5-*p*-dimethylaminophenyl groups. Based on the single crystal structure of **QLD-BDP**, its aggregation state is found to be the *J*-aggregation [33–37]. This new molecule absorbs and emits in NIR-II region, with good photothermal conversion efficiency (50.5%). **QLD-BDP** nanoparticles (**QLD-BDP**-NPs) could localize in mitochondria. **QLD-BDP-**NPs inhibited the growth of 4T1 multicellular spheroids (MCSs) by light irradiation, internalized into tumor rapidly and could not be excreted from the cells for 12 h. **QLD-BDP-**NPs could cause the complete destruction of 4T1 MCSs and had a PTT effect.

* Corresponding authors.
E-mail addresses: xdjiang@syuct.edu.cn (X.-D. Jiang), dujj@dlut.edu.cn (J. Du).
[1] These authors contributed equally to this work.

https://doi.org/10.1016/j.cclet.2024.109735
1001-8417/

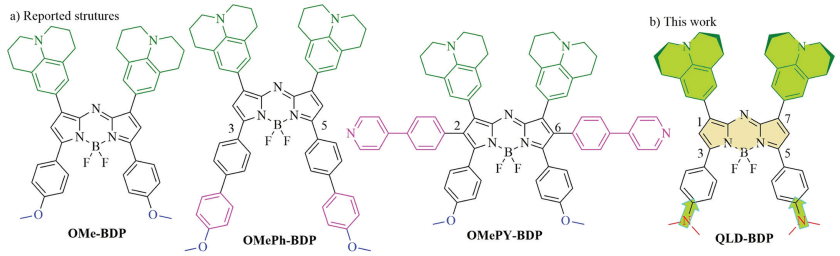

Fig. 1. Design of aza-BODIPY **QLD-BDP** with 1,7-julolidine-3,5-NMe_2 groups for aggregation.

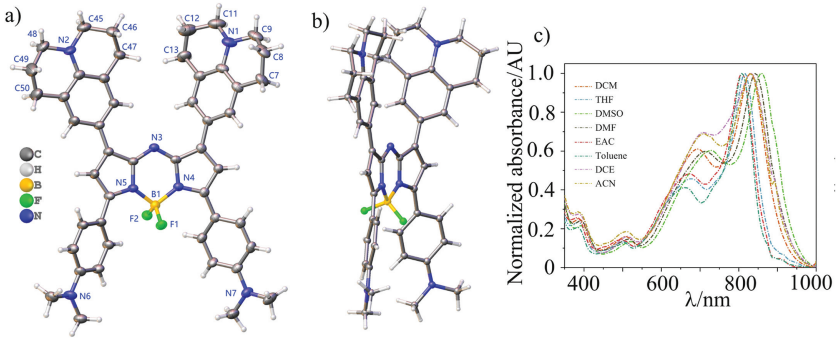

Fig. 2. Oak ridge thermal ellipsoid plot (ORTEP) views of **QLD-BDP** (CCDC: 2299513) (displacement ellipsoids at the 30% probability level). (a) Front, (b) side views of the molecular structure. Selected bond lengths (Å) and angles (°): N4-B1, 1.547(6); N5-B1: 1.546(6); B1-F1: 1.375(6); B1-F2: 1.425(6); N4-B1-N5: 106.2(4); F1-B1-F2: 110.1(4). (c) Normalized absorption of **QLD-BDP** in different solvents, respectively.

Since it is of great value to construct a NIR absorbing dye aza-BODIPY, julolidine at 1,7-sites and *p*-dimethylaminophenyl group at 3,5-sites in aza-BODIPY system serves as a donor for the aza-BODIPY nucleus as a receptor, constructing a powerful D-A structural molecule. Using hexahydropyrido[3,2,1-*ij*]quinoline-9-carbaldehyde and 1-(4-(dimethylamino)phenyl)ethanone as the starting material, we successfully synthesized aza-BODIPY **QLD-BDP** in 14% total yield (Fig. 1b and Scheme S1 in Supporting information). According to the ^{1}H NMR spectra, three different sets of -CH_2- peaks and one set of -CH_3 peaks can be clearly observed, confirming this molecular structure. Furthermore, we were fortunate to obtain the X-ray crystal of **QLD-BDP**, which is the first structure of julolidine-containing aza-BODIPY to date (Fig. 2a). Based on the single crystal structure, we found that the -CH_2- groups, directly connecting to phenyl groups (C7, C13, C47 and C50) and the sp^2 hybridized N (C9, C11, C45 and C48), maintain a coplanar structure with the phenyl groups (Fig. 2a). We also found that the four -CH_2- groups in the middle sites (C8, C12, C46 and C49) were all tilted in the same direction, without adopting the distribution pattern on both sides of the phenyl plane. The angle of C48-C49-C50 is 114.3°, far deviating from the ideal value of 109.5°, indicating that C49 is closer to the plane mentioned above. However, the other three -CH_2- groups (C8, C12, and C46) basically adopt the ideal sp^3 hybrid structure. The B-F distances (1.375 and 1.425 Å) in **QLD-BDP** were found to be longer than that of the corresponding aza-BODIPY with 1,7-diphenyl groups (1.391 and 1.389 Å) by 0.036 Å [24,38], owing to the strong electron-donating effect. The N4–B1–N5 and F1–B1–F2 angles were 106.2° and 110.1° respectively, indicating the boron atom in the center is a seriously distorted sp^3 configuration. Therefore, due to the introduction of julolidine at 1,7-sites, the aza-BODIPY nucleus exhibits the significant distortion, and the overall molecule appears a bowl shaped structure (Fig. 2b and Fig. S1 in Supporting information).

Next, we gained insight into spectral characteristics of **QLD-BDP** in different solvents. It found that the maxima absorption of **QLD-BDP** in various solvents ranged from 810 nm to 862 nm, with a broad full width at half maxima (FWHM) and a high molar extinction coefficient (for instance, $\varepsilon = 166{,}000\ \mathrm{L\ mol^{-1}\ cm^{-1}}$ in CH_2Cl_2) (Fig. 2c and Table S1 in Supporting information). Among them, the maxima absorption of **QLD-BDP** in small polar solvent toluene is 810 nm, while **QLD-BDP** in large polar solvent DMSO is 862 nm with FWHM of 230 nm (Table S1). Subsequently, singlet oxygen ($^1O_2$) generation of **QLD-BDP** to inspect the intersystem crossing (ISC) process was investigated (Fig. S2 in Supporting information). By using 1,3-diphenylisobenzofuran (DPBF) as a $^1O_2$ indicator, the efficiency of $^1O_2$ generation was evaluated by detecting the decrease of DPBF indicator absorbance at 416 nm [39–43]. Based on the decay lines at 416 nm, the $^1O_2$ yields of **QLD-BDP** were very low and near to be 0, indicating that ISC is basically prohibited.

Because we obtained the data of weak fluorescence (Table S1) and singlet oxygen generation of this novel dye **QLD-BDP**, such information urges us to further explore the insight into the photothermal conversion capacity. To enhance the biocompatibility and the water solubility of **QLD-BDP** for photoimaging and phototherapy in biological system, **QLD-BDP** and amphipathic polymer material 1,2-distearoyl-*sn*–glycero–3-phosphoethanolamine-*N*-[methoxy(polyethylene glycol)–2000] (DSPE-PEG_{2000}) were self-assembled into dye **QLD-BDP** nanoparticles (**QLD-BDP-**NPs) (Fig. 3a) [44–46]. To understand the molecular design concept, the molecular packing mode of **QLD-BDP** *via* single crystal structure analysis was firstly investigated (Fig. 3b). In the single-crystal structure, the π-π interactions between one julolidine group (green) and another julolidine group (green), between the julolidine group (green) and the dimethylaminophenyl group (yellow) (Fig. S1), facilitate the aggregation packing mode. While dye **QLD-BDP** adopts coplanar inclined arrangement of its transition dipole, a slip angle of 35° is clearly observed (Fig. 3b). This arrangement of aggregate is in great agreement with Kasha's molecular exciton model, and corresponds to textbook cases of *J*-type ($\theta < 54.7°$) packing for **QLD-BDP** (Fig. 3b) [47–49]. Dynamic light scattering (DLS) of **QLD-BDP**-NPs showed a suitable hydrodynamic diameter (30–110 nm) in Fig. 3c, and the average hydrodynamic diameter and the polydispersity index (PDI) were about 81.36 nm and 0.173.

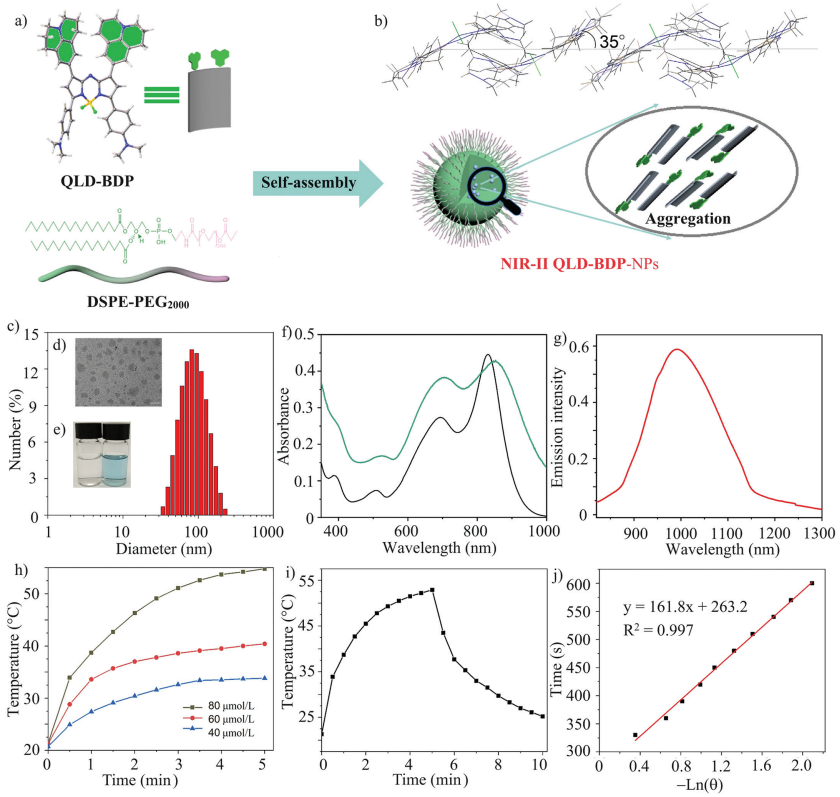

Fig. 3. (a) Self-assembly of **QLD-BDP-**NPs. (b) Molecular packing diagram of side view for **QLD-BDP**. (c) DLS of **QLD-BDP-**NPs in aqueous solution. (d) TEM of **QLD-BDP-**NPs in aqueous solution. Scale bar: 100 nm. (e) Photo of pure water and **QLD-BDP-**NPs in water. (f) Absorption of 2 μmol/L **QLD-BDP-**NPs (black curve) in CH_2Cl_2 and 10 μmol/L **QLD-BDP-**NPs in water (green curve). (g) Fluorescence of 10 μmol/L **QLD-BDP-**NPs in water. λ_{ex} = 808 nm; laser source. (h) Temperature changes of **QLD-BDP-**NPs at different concentrations (40–80 μmol/L) under 808 nm laser irradiation (0.8 W/cm^2). (i) Temperature response curves of **QLD-BDP-**NPs in aqueous solutions under irradiation and naturally cooling. (j) Linear fitting of −Lnθ and time.

The azury **QLD-BDP**-NPs in aqueous solution stood for one week (Figs. 3d and e). Due to the aggregate effect (Fig. 3a and Fig. S3 in Supporting information), the absorption maximum (λ_{abs}= 866 nm) of **QLD-BDP**-NPs in aqueous solution bathochromically shifted 36 nm and its absorption band covered the NIR region (600–1000 nm) and became wider (Fig. 3f), comparing to those (λ_{abs}= 830 nm) of **QLD-BDP** in CH_2Cl_2. Additionally, **QLD-BDP-**NPs emit fluorescence (λ_{em} = 998 nm, ϕ_f = 0.001) when excited at 808 nm, and a peak belt covers a NIR-II range of 1000–1300 nm (Fig. 3g).

Next, photothermal conversion efficiency of **QLD-BDP-**NPs was measured. The temperatures of **QLD-BDP-**NPs (40, 60 and 80 μmol/L) in aqueous solution were found to be increased gradually under light radiation (0.8 W/cm^2, 5 min) (Fig. 3h). Moreover, the heating effect is proportional to the concentration of **QLD-BDP-**NPs. Under 80 μmol/L of **QLD-BDP-**NPs and 0.8 W/cm^2 light radiation, the solution can be quickly heated to 55.1 °C in 5 min (Fig. S4 in Supporting information). The higher temperature-elevated performance is associated with intense light radiation power (0.4–0.8 W/cm^2) in Fig. S5 (Supporting information). So, the photothermal effect was positively related to concentration and light power density, indicating that the heat generation could be controlled. Natural cooling for 5 min after 5 min light radiation could reduce the temperature almost to room temperature (Fig. 3i). Based on the corresponding relationship between cooling time and −Lnθ (Fig. 3j), the photothermal conversion efficiency (η) was calculated as 50.5%, which was in agreement with that previously reported for aza-BODIPY derivatives [19]. Furthermore, we tested the temperature changes of five heating-cooling cycles, which showed that **QLD-BDP-**NPs had good photothermal stability, and temperature changes of the five cycles were similar (Fig. S6 in Supporting information).

The colocalization of **QLD-BDP-**NPs with Lyso-Tracker Green (LTG), ER-Tracker Green (ETG) or Mito-Tracker Green (MTG) in 4T1 cells was investigated, respectively (Fig. 4) [50,51]. Colocalization experiments showed that the green fluorescence signal of LTR and ETR overlapped poorly with the red fluorescence signal of **QLD-BDP-**NPs, with low Pearson coefficients of 0.775 and 0.677, respectively (Figs. 4a and b). However, when 4T1 cells were labeled with **QLD-BDP-**NPs and MTR, colocalization experiments confirmed that the green fluorescence of MTR overlapped well with the red fluorescence of **QLD-BDP-**NPs, and the Pearson coefficient reached 0.890 (Fig. 4c). These results indicated better specific imaging and localization ability of **QLD-BDP-**NPs for mitochondria than lysosome and endoplasmic reticulum.

MTT assay was employed to further evaluate the effect of different concentrations of **QLD-BDP-**NPs on the viability of 4T1 tumor cells under darkness and 850 nm laser irradiation (0.2 W/cm^2, 8 min). As shown in Fig. S7 (Supporting information), under darkness the inhibition of **QLD-BDP-**NPs on the activity of tumor cells gradually increased with the increase of **QLD-BDP-**NPs concentration. Under laser irradiation, cell viability decreased significantly, and cell viability was only 3.01% in present of 40 μg/mL **QLD-BDP-**NPs. The experimental results showed that **QLD-BDP-**NPs had low dark toxicity and high phototoxicity. Furthermore, to investigate the triggering mechanism of **QLD-BDP**-NPs on cancer cells, flow cytometry was applied to explore relevant apoptosis in 4T1 cells (Fig. S8 in Supporting information). The treatment with **QLD-BDP-**NPs plus laser irradiation obviously caused apoptosis in cancer cells, and the percentage of apoptotic cells increased from 7.24%

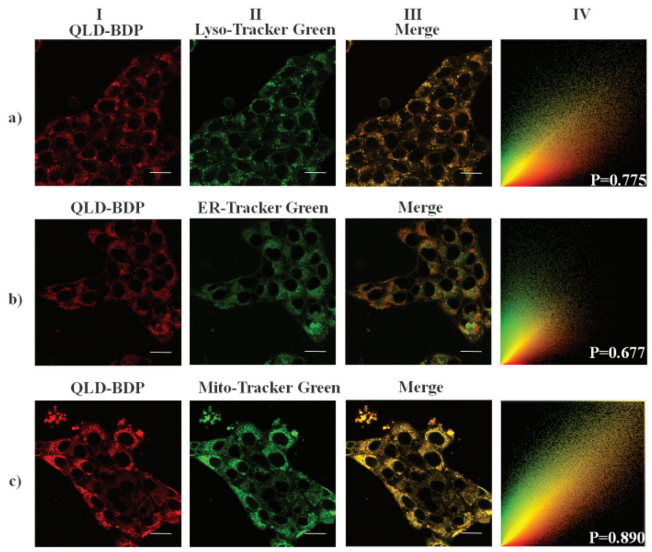

Fig. 4. Colocalization of **QLD-BDP-**NPs with LTG, ETG or MTG for (a) lysosome, (b) endoplasmic reticulum, and (c) mitochondria in 4T1 cells (**QLD-BDP-**NPs: λ_{ex} =640 nm, λ_{em} = 650–750 nm; Tracker: λ_{ex} = 488 nm, λ_{em} = 500–600 nm; Scale bar: 20 μm). Cells were labeled with **QLD-BDP-**NPs (20 μg/mL) and LTG (1.0 μmol/L), ETG (1.0 μmol/L) or MTG (1.0 μmol/L), respectively. (I) **QLD-BDP-**NPs labeled with red fluorescence; (II) Organelles labeled with green fluorescence; (III) Superposition of red and green fluorescence in yellow, indicating colocalization; (IV) Pearson coefficient of pixel intensity.

to 50.67%, whereas cells treated with **QLD-BDP-**NPs or light alone showed a lower rate of apoptosis.

The uptake and permeation ability of drugs in MCSs is an important factor affecting their therapeutic effect on tumors [52–54]. Therefore, based on mouse breast cancer 4T1 cells, a 3D multicellular spheroid tumor model *in vitro* was established to study cell uptake. After 12 h of exposure to **QLD-BDP-**NPs, imaging of MCSs was performed using single photon fluorescence confocal microscopy (CLSM). As the Z-axis stacking depth extends, **QLD-BDP-**NPs were found to exhibit a clear process of infiltrating from the edge to the inside (Fig. 5a), stimulating their tracking and imaging *in vitro*. So, **QLD-BDP-**NPs could internalize into tumor rapidly and could not be excreted from the cells for 12 h. To evaluate the phototoxicity of **QLD-BDP-**NPs on MCSs, the MCSs of 4T1 cells were treated with 20 and 40 μg/mL **QLD-BDP-**NPs in phosphate buffered saline (PBS), and the culture medium was changed every other day (Fig. 5b). After 12 h of cultivation, the MCSs were formed. Then, the MCSs were further cultured under laser irradiation (0.3 W/cm^2, 900 s) or darkness for two days to observe the morphological changes. Compared with the control group without laser irradiation, 20 or 40 μg/mL **QLD-BDP-**NPs have a slight inhibitory effect on the growth of MCSs. Under laser irradiation, 20 or 40 μg/mL **QLD-BDP-**NPs have a significant inhibitory effect on the growth of MCSs. Especially, MCSs treated with 40 μg/mL **QLD-BDP-**NPs exhibited more significant disintegration, demonstrating higher PTT efficiency. Therefore, the unique ability of **QLD-BDP-**NPs to inhibit the growth of MCSs by light irradiation indicates that **QLD-BDP-**NPs have the potential to inhibit solid tumors *in vivo*.

To further test the phototherapy effect of **QLD-BDP-**NPs, MCSs were treated with 40 μg/mL **QLD-BDP-**NPs, and then stained with calcein AM (green) and propidium iodide (PI, red) dyes in the dark group and the light group, respectively. Green fluorescence represents living cells, while red fluorescence represents dead cells. As shown in Fig. 5c, it is once again demonstrated that **QLD-BDP-**NPs have a slight inhibitory effect on the growth of 4T1 MCSs without laser irradiation. Under NIR laser irradiation (850 nm, 0.3 W/cm^2, 900 s), a strong red fluorescence was obviously observed, indicating that **QLD-BDP-**NPs caused the complete destruction of 4T1 MCSs.

In conclusion, utilizing hexahydropyrido[3,2,1-*ij*]quinoline-9-carbaldehyde and 1-(4-(dimethylamino)phenyl)ethanone as the starting material, we successfully synthesized aza-BODIPY **QLD-BDP** in 14% total yield. Based on the single crystal structure, due to the introduction of julolidine at 1,7-sites, the aza-BODIPY nucleus exhibits the significant distortion, and the overall molecule appears a bowl shaped structure. Owing to the aggregation effect, the absorption maximum (λ_{abs} = 866 nm) of **QLD-BDP-**NPs in aqueous solution bathochromically shifted 36 nm and the absorption band covered the NIR region (600–1000 nm) and became wider. **QLD-BDP-**NPs emit fluorescence (λ_{em} = 998 nm, ϕ_f = 0.001) when excited at 808 nm, and a peak belt covers a NIR-II range of 1000–1300 nm. The PCE of the self-assembled **QLD-BDP-**NPs by aggregate can reach 50.5%. **QLD-BDP-**NPs have better specific imaging and localization ability for mitochondria than lysosome and endoplasmic reticulum. **QLD-BDP-**NPs could internalize into tumor rapidly and could not be excreted from the cells. **QLD-BDP-**NPs caused the complete destruction of 4T1 MCSs and possessed a PTT effect.

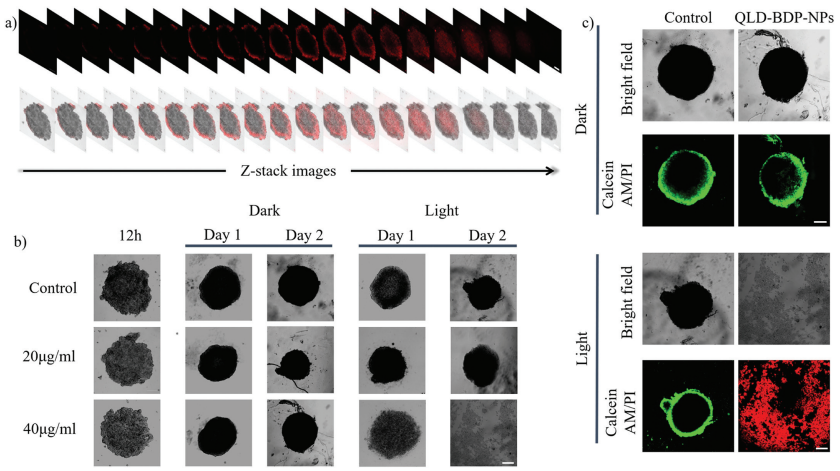

Fig. 5. (a) Imaging of MCSs of 4T1 cells (λ_{ex} =640 nm, λ_{em} = 650–750 nm). (b) CLSM analysis image of 4T1 MCSs. MCSs were cultured in a medium PBS containing 20 or 40 μg/mL **QLD-BDP-**NPs. Use a laser at 850 nm (0.3 W/cm^2, 900 s) for light irradiation. The images of the spherical formation for 12 h before irradiation were recorded, and the images of the first and second days with or without light irradiation were recorded. (c) Live/dead cell imaging of 4T1 MCS treated with **QLD-BDP-**NPs under dark and light irradiation (850 nm, 0.3 W/cm^2, 900 s), respectively. Scale bar: 200 μm.

Declaration of competing interest

The authors declare that they have no known competing financial interests or personal relationships that could have appeared to influence the work reported in this paper.

Acknowledgments

This work was supported by the National Natural Science Foundation of China (Nos. 22078201, U1908202), Liaoning & Shenyang Key Laboratory of Functional Dye and Pigment (Nos. 2021JH13/10200018, 21–104–0–23).

Supplementary materials

Supplementary material associated with this article can be found, in the online version, at doi:10.1016/j.cclet.2024.109735.

References

[1] S. Diao, G. Hong, A.L. Antaris, et al., Nano Res. 8 (2015) 3027–3034.
[2] G. Hong, A.L. Antaris, H. Dai, Nat. Biomed. Eng. 1 (2017) 0010.
[3] Z. Lei, F. Zhang, Angew. Chem. Int. Ed. 60 (2021) 16294–16308.
[4] C. Li, G. Chen, Y. Zhang, et al., J. Am. Chem. Soc. 142 (2020) 14789–14804.
[5] S. Wang, H. Shi, L. Wang, et al., J. Am. Chem. Soc. 144 (2022) 23668–23676.
[6] J. Cao, B. Zhu, K. Zheng, et al., Front. Bioeng. Biotechnol. 7 (2020) 487.
[7] S. He, J. Song, J. Qu, et al., Chem. Soc. Rev. 47 (2018) 4258–4278.
[8] G. Hong, J.C. Lee, J.T. Robinson, et al., Nat. Med. 18 (2012) 1841–1846.
[9] G. Hong, Y. Zou, A.L. Antaris, et al., Nat. Commun. 5 (2014) 4206.
[10] Z. Hu, C. Fang, B. Li, et al., Nat. Biomed. Eng. 4 (2019) 259–271.
[11] Y. Jiang, K. Pu, Adv. Biosyst. 2 (2018) 1700262.
[12] M.H. Lee, A. Sharma, M.J. Chang, et al., Chem. Soc. Rev. 47 (2018) 28–52.
[13] Q. Shen, S. Wang, N.-D. Yang, et al., J. Lumin. 225 (2020) 117338.
[14] A.M. Smith, M.C. Mancini, S. Nie, Nat. Nanotechnol. 4 (2009) 710–711.
[15] S. Zhu, B.C. Yung, S. Chandra, et al., Theranostics 8 (2018) 4141–4151.
[16] Y. Zhang, Y. Jia, S. Zhu, SmartMat 5 (2024) e1245.
[17] T. Li, T. Meyer, R. Meerheim, et al., J. Mater. Chem. A 5 (2017) 10696–10703.
[18] Y. Liu, D. Gao, M. Xu, et al., J. Biophotonics 12 (2018) e201800237.
[19] Z. Shi, X. Han, W. Hu, et al., Chem. Soc. Rev. 49 (2020) 7533–7567.
[20] M. Strobl, A. Walcher, T. Mayr, et al., Anal. Chem. 89 (2017) 2859–2865.
[21] M. Liu, S. Ma, M. She, et al., Chin. Chem. Lett. 30 (2019) 1815–1824.
[22] M. Kaur, A. Janaagal, N. Balsukuri, et al., Coord. Chem. Rev. 498 (2024) 215428.
[23] Y. Wang, D. Zhang, K. Xiong, et al., Chin. Chem. Lett. 33 (2022) 115–122.
[24] Y. Su, Q. Hu, D. Zhang, et al., Chem. Eur. J. 28 (2022) e202103571.
[25] S.Z. Wang, Y. Guo, X. Zhang, et al., Adv. Funct. Mater. 33 (2023) 2303328.
[26] A.M. Scott, T. Miura, A.B. Ricks, et al., J. Am. Chem. Soc. 131 (2009) 17655–17666.
[27] H. Dang, D. Yin, Y. Tian, et al., J. Mater. Chem. B 10 (2022) 5279–5290.
[28] K. Okino, S. Hira, Y. Inoue, et al., Angew. Chem. Int. Ed. 56 (2017) 16597–16601.
[29] G. Wu, F. Kong, J. Li, et al., J. Power Sources 243 (2013) 131–137.
[30] L. Bai, P. Sun, Y. Liu, et al., Chem. Commun. 55 (2019) 10920–10923.
[31] Z. Shi, H. Bai, J. Wu, et al., Research 6 (2023) 0169.
[32] C. Li, Y. Xu, L. Tu, et al., Chem. Sci. 13 (2022) 6541–6549.
[33] F. Würthner, T.E. Kaiser, C.R. Saha-Möller, Angew. Chem. Int. Ed. 50 (2011) 3376–3410.
[34] M.H.Y. Cheng, K.M. Harmatys, D.M. Charron, et al., Angew. Chem. Int. Ed. 58 (2019) 13394–13399.
[35] X. Zhang, H. Wang, D. Li, et al., Macromolecules 53 (2020) 3747–3755.
[36] Y. Qu, W. Jin, Y. Wan, et al., Chin. Chem. Lett. 35 (2024) 108493.
[37] N. Yang, S. Song, M.H. Akhtar, et al., J. Mater. Chem. B 11 (2023) 9712–9720.
[38] A. Gorman, J. Killoran, C. O'Shea, et al., J. Am. Chem. Soc. 126 (2004) 10619–10631.
[39] J.N. Schrauben, J.L. Ryerson, J. Michl, et al., J. Am. Chem. Soc. 136 (2014) 7363–7373.
[40] W. Zhang, B. Li, H. Ma, et al., ACS Appl. Mater. Interfaces 8 (2016) 21465–21471.
[41] M.L. Agazzi, M.B. Ballatore, E. Reynoso, et al., Eur. J. Med. Chem. 126 (2017) 110–121.
[42] Z. Li, C. Liu, H. Abroshan, et al., ACS Catal. 7 (2017) 3368–3374.
[43] X. Wang, Y. Yu, K. Cheng, et al., Mikrochim. Acta 186 (2019) 842.
[44] S. Jiang, X. Wang, Z. Zhang, et al., Int. J. Nanomedicine 11 (2016) 5505–5518.
[45] J. Chen, A.C. Sedgwick, S. Sen, et al., Chem. Sci. 12 (2021) 9916–9921.
[46] H. Ning, Y. Yang, C. Lv, et al., Nano Res. 16 (2023) 12294–12303.
[47] Y.H. Kim, D.H. Jeong, D. Kim, et al., J. Am. Chem. Soc. 123 (2000) 76–86.
[48] T.L.C. Jansen, Chem 5 (2019) 3010–3012.
[49] Y. Li, T. Ma, H. Jiang, et al., Angew. Chem. Int. Ed. 61 (2022) e202203093.
[50] C. Li, H. Ge, D. Zhang, et al., Sens. Actuator. B: Chem. 344 (2021) 130213.
[51] J. Huang, X. Sun, Y. Wang, et al., Ecotoxicol. Environ. Saf. 264 (2023) 115447.
[52] M. Azharuddin, K. Roberg, A.K. Dhara, et al., Sci. Rep. 9 (2019) 20066.
[53] M. Wan, Q. Wang, X. Li, et al., Angew. Chem. Int. Ed. 59 (2020) 14458–14465.
[54] Y. Lu, F. Xu, Y. Wang, et al., Biomaterials 278 (2021) 121167.